

Exploration of the Correlation between Solvation Dynamics and Internal Dynamics of a Protein

Anjali Jha,[‡] Kunihiko Ishii,[§] Jayant B. Udgaonkar,^{*,§,||} Tahei Tahara,^{*,§} and G. Krishnamoorthy^{*,‡}

[‡]Department of Chemical Sciences, Tata Institute of Fundamental Research, Mumbai 400005, India, [§]Molecular Spectroscopy Laboratory, Advanced Science Institute (ASI), RIKEN, Wako, Saitama 351-0198, Japan, and ^{||}National Centre for Biological Sciences, Tata Institute of Fundamental Research, Bangalore 560065, India

Received September 7, 2010; Revised Manuscript Received December 5, 2010

ABSTRACT: Protein function is intimately related to the dynamics of the protein as well as to the dynamics of the solvent shell around the protein. Although it has been argued extensively that protein dynamics is slaved to solvent dynamics, experimental support for this hypothesis is scanty. In this study, measurements of fluorescence anisotropy decay kinetics have been used to determine the motional dynamics of the fluorophore acrylodan linked to several locations in a small protein barstar in its various structural forms, including the native and unfolded states as well as the acid and protofibril forms. Fluorescence upconversion and streak camera measurements have been used to determine the solvation dynamics around the fluorophore. Both the motional dynamics and solvent dynamics were found to be dependent upon the location of the probe as well as on the structural form of the protein. While the (internal) motional dynamics of the fluorophore occur in the 0.1–3 ns time domain, the observed mean solvent relaxation times are in the range of 20–300 ps. A strong positive correlation between these two dynamical modes was found in spite of the significant difference in their time scales. This observed correlation is a strong indicator of the coupling between solvent dynamics and the dynamics in the protein.

It is well recognized that proteins and other biological macromolecules are dynamic entities and that the dynamics of various segments play a major role in their function (1–3). The notion that water plays a dominant role in dictating the dynamics has gained importance in recent years. The side chains of amino acid residues on the surface of a protein are hydrated, resulting in several layers of bound water whose properties are the object of intense research efforts (4–9).

Frauenfelder and co-workers have championed the notion that protein dynamics and, hence, function are “slaved” to solvent fluctuations (8). They have proposed the presence of two types of equilibrium fluctuations, namely, α and β fluctuations, in proteins, in analogy to the fluctuations seen in glass-forming liquids (10). These fluctuations have been hypothesized to originate from fluctuations in the bulk solvent (α fluctuations) and in the hydration shell around the protein (β fluctuations). β fluctuations are thought to control internal motions of proteins. A recent experimental demonstration of a correlation between the β fluctuations and functional dynamics supports this hypothesis (8).

In this work, we address the question whether the “solvation” dynamics, as monitored by the time-dependent dynamic Stokes

shift (TDSS)¹ measurements, is coupled to the local motional dynamics of the protein monitored by time-resolved fluorescence anisotropy measurements. Barstar, an 89 amino acid protein which has been extensively used as a model system for protein folding and misfolding studies (11–13), was site-specifically labeled with the fluorophore acrylodan at different positions along the sequence (Figure 1). Barstar forms soluble aggregates (the acid form or A form) at pH < 3, which have been studied by fluorescence and NMR and characterized as 160 kDa molten globule-like structures (14, 15). The A form formed at low pH can be transformed into fibrillar aggregates at elevated temperatures (11, 16, 17). The structure of protofibrils (PF) has been characterized using time-resolved fluorescence spectroscopy (17). Each singly labeled protein was studied in four structural forms, including the native protein (N), the unfolded protein (U), a soluble oligomer (A form), and the protofibrillar form (PF). The large number of samples enabled us to explore the correlations between “solvation” dynamics and local protein dynamics. Fluorescence upconversion and streak camera detection were used to study the solvation dynamics through TDSS, and the motional dynamics of the fluorophore was measured from the fluorescence anisotropy decay kinetics. Our results clearly bring out the positive correlation between TDSS and protein dynamics.

METHODS

Protein Expression and Purification. The mutant proteins of barstar Cys3, Cys25, Cys40, Cys62, Cys82, and Cys89 each with a single cysteine and single tryptophan residue (W53) were purified as described previously (18).

Preparation of Labeled Protein. All of the mutant proteins were labeled with the thiol labeling probe acrylodan in 5 M urea

*To whom correspondence should be addressed. J.B.U.: e-mail, jayant@ncbs.res.in; telephone, 91-80-23666150; fax, 91-80-23636662. T.T.: e-mail, tahei@riken.jp; telephone, +81-48-467-4592; fax, +81-48-467-4539. G.K.: e-mail, gk@tifr.res.in; telephone, +91-22-2278 2301; fax, +91-22-2280 4610/4611.

Abbreviations: acrylodan, 6-acryloyl-2-(dimethylamino)naphthalene; 1,5-IAEDANS, 5-(((2-iodoacetyl)amino)ethyl)amino)naphthalene-1-sulfonic acid; IRF, instrument response function; PF, protofibril form; N, native protein; SC, streak camera; TDSS, time-dependent dynamic Stokes shift; TRES, time-resolved emission spectra; U, unfolded protein; UC, upconversion.

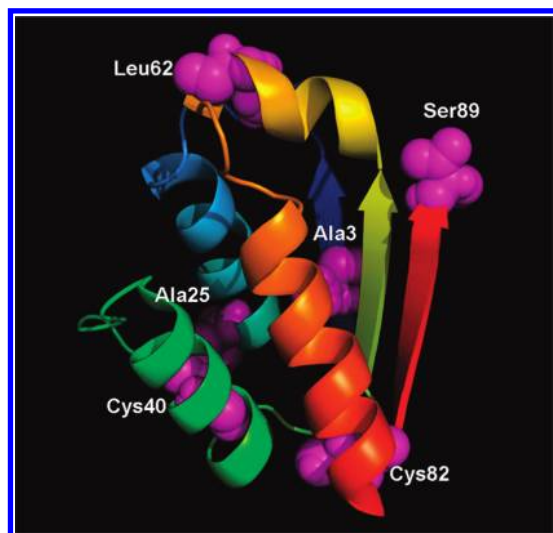


FIGURE 1: Structure of the native state of barstar. The locations of the six different residues which were mutated to cysteine are shown. The structure was drawn using PyMOL and the PDB file 1A19.

and 20 mM Tris-HCl at pH 8 using a 20-fold molar excess of the dye in the dark. This reaction mixture was kept at room temperature for 2 h. After the labeling reaction was complete, the labeled protein was separated from free dye and urea by passing the reaction mixture through a PD-10 column (Pharmacia). A similar procedure was followed to obtain IAE-DANS-labeled mutant proteins for the acrylamide quenching experiments. The extent of labeling was checked as described earlier (12) and was found to be >95% for all of the mutant proteins. It was shown that labeling with acrylodan does not modify the native structure or stability of the protein significantly by measurement of equilibrium unfolding curves in the presence of the denaturant, urea. The midpoints of the equilibrium transitions of the labeled proteins were found to be within 5% of those obtained for the corresponding unlabeled proteins by monitoring the fluorescence of either the tryptophan or the acrylodan label. A small slope was observed in the native protein baseline region of the unfolding curve monitored by acrylodan fluorescence (data not shown), which could indicate local melting of structure around the acrylodan adduct. The main motivation of the present work is, however, to explore the correlation between the intrinsic motional dynamics of the fluorophore attached to various locations in the protein with the solvation dynamics felt around the fluorophore at that location and in a particular structural form of the protein. Hence any small local perturbation induced by the fluorophore is unlikely to be of major concern for the problem being addressed in this work.

Preparation of Various States of Labeled Mutants from Native Mutant Proteins. Purified labeled protein was concentrated using a Millipore filter (5 kDa cutoff). A stock solution of 500 μ M protein in 20 mM Tris-HCl buffer (pH 8.0) was made. The concentration was checked as described above. The stock solution of the 500 μ M labeled native protein was diluted 10-fold into the 50 mM glycine buffer (pH 2.7) to give 50 μ M of the A form. The A form was incubated at room temperature for 30 min. The PF were formed by heat (70 °C) treatment for 2.5 h of the A form in a water bath. The PF were brought back to room temperature after heating and incubated at room temperature for 10–15 min prior to data collection. The aggregated form of Cys25-acrylodan showed very high photobleaching, due to some unknown reason, and thus, these samples could not be used for

data collection and were discarded. Labeled mutant protein was unfolded in 6 M GdnHCl and incubated at room temperature for 2 h prior to data collection.

Time-Resolved Fluorescence Measurements. (A) *Fluorescence Upconversion Measurement.* The experimental setup for the femtosecond fluorescence upconversion measurement is essentially the same as that described previously (19). The excitation source was 760 nm obtained from a mode-locked Ti:sapphire laser (Coherent; MIRA) with a typical pulse duration of 105 fs. This fundamental pulse was frequency doubled to the second harmonic pulse at 380 nm by using a β -BaB₂O₄ crystal (0.2 mm thickness). The generated second harmonic pulse was used for excitation of the labeled protein in a microcuvette of dimension 10 mm \times 0.5 mm. The residual fundamental pulse of 760 nm after the second harmonic generation was used as a gate pulse for the upconversion process. The fluorescence from the sample was collected and focused into another β -BaB₂O₄ mixing crystal with the use of an aluminum-coated elliptic mirror. A cutoff filter was placed between the mirror and the mixing crystal to block the excitation light. The fluorescence was upconverted by sum-frequency generation with the gate pulse in the mixing crystal. The upconverted signal was separated from other light by an iris, band-pass filters, and a monochromator (HR-320; Jobin Yvon), and then it was detected by a photon-counting photomultiplier with a counter (SR-400; Stanford Research Systems). The time resolution was evaluated as \sim 200 fs by the upconversion measurement of the Raman signal from the solvent. The fluorescence was detected at the magic angle (54.7°) by rotating the excitation polarization with respect to the gate polarization. Fluorescence transient decays of acrylodan coupled to the single cysteine in each of the various mutant proteins were collected up to the 50 ps time range at 11 gated wavelengths, i.e., 450–600 nm, at intervals of 15 nm each. As the time scale of the solvation process may occur in the femtosecond to several nanosecond time domain, this technique is extremely useful to capture the initial ultrafast decay of the solvation process. Streak camera measurement was done in order to measure the solvation on longer time scale.

(B) *Streak Camera Measurements.* Picosecond time-resolved fluorescence of all acrylodan-labeled mutants was collected by the use of a highly sensitive streak camera system with 20 ps time resolution. The elaborate description of the experimental setup has been given elsewhere (20). In brief, a femtosecond laser pulse with a 1 kHz repetition rate Ti:sapphire regenerative amplifier was used. A minor part of the fundamental was used to trigger the streak camera, and a major part was frequency doubled to 380 nm using a BBO crystal. This 380 nm output was used to excite the sample in a cuvette of dimension 10 mm \times 0.5 mm, and the subsequent fluorescence was focused on a spectrograph with the help of lens. A polarizer was set in between the lens and the spectrograph at the magic angle along with an emission filter to reject the scattered light. The wavelength-resolved output of the spectrograph was focused on the photocathode of the streak camera (Hamamatsu C4334). The streak camera converted the temporal profile to a spatial profile and detected the streak image. Finally, the image was analyzed to get picosecond-resolved fluorescence decays at different wavelengths. The time resolution was evaluated to be \sim 20 ps for the Raman signal from the solvent.

(C) *Time-Resolved Fluorescence Anisotropy Measurements.* Time-resolved fluorescence intensity and anisotropy decay kinetic experiments were carried out using a Ti-sapphire

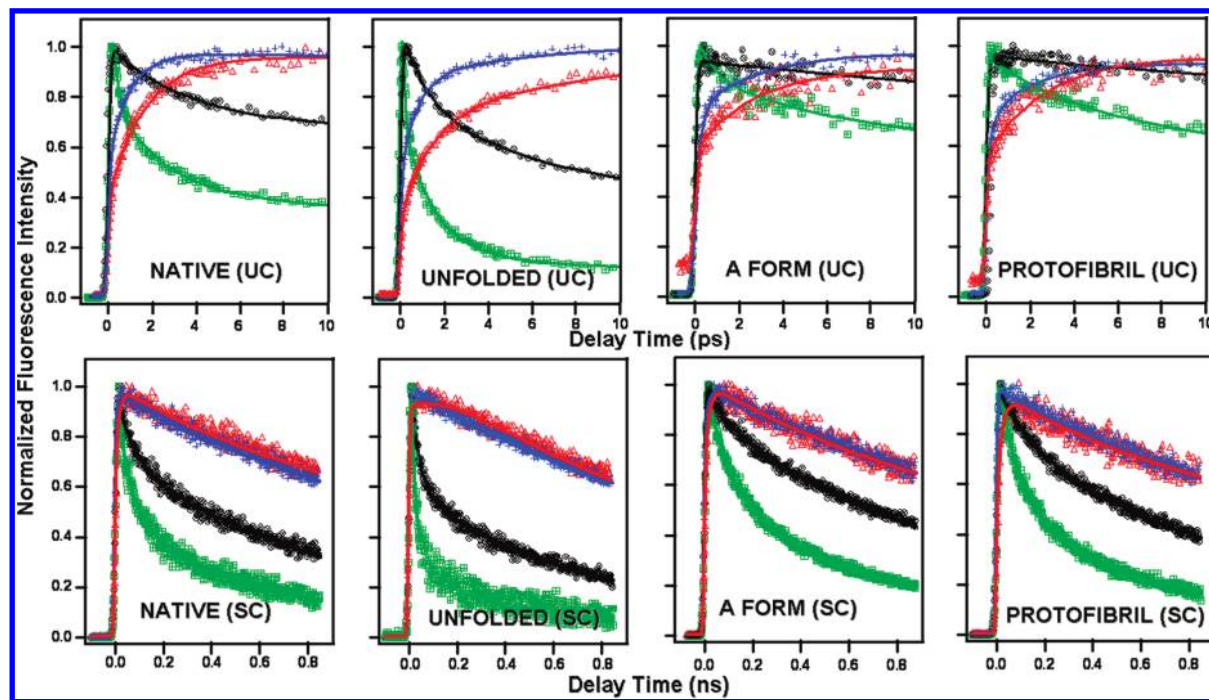


FIGURE 2: Normalized femto/picosecond-resolved fluorescence transients measured by fluorescence upconversion and streak camera. Normalized femto/picosecond-resolved fluorescence transients of the Cys82-acrylodan mutant form for four emission wavelengths, 450 (green) 480 (black), 525 (blue), and 570 (red) nm, in the native state, the unfolded state, the A form, and the PF form, were captured by fluorescence upconversion (UC) in the short time range and streak camera (SC) in the long time ranges. The symbols denote the actual values of the normalized fluorescence intensity, and the solid lines denote the best fit to multiexponential decays.

picosecond laser and a time-correlated single-photon-counting (TCSPC) setup, coupled to a microchannel plate photomultiplier as described earlier (11). Pulses of 1 ps duration of 820 nm radiation from the Ti-sapphire laser were frequency doubled to 410 nm using a frequency doubler (GWU; Spectra Physics). For all of the time-resolved measurements, samples were excited at 410 nm at a pulse repetition rate of 4 MHz, and emission was measured at 525 nm. The instrument response function (IRF) was obtained at 410 nm using a very dilute colloidal suspension of dried nondairy coffee whitener. The width (FWHM) of the IRF was ~ 40 ps. The decay was deconvoluted with respect to the IRF and analyzed using a sum of discrete exponentials as described in the Data Analysis section. For the fluorescence lifetime measurements, peak counts of 10000 were collected with the emission polarizer oriented at the magic angle (54.7°) with respect to the excitation polarizer. For time-resolved anisotropy measurements, the emission data were collected at 0° (parallel fluorescence intensity I_{\parallel}) and 90° (perpendicular fluorescence intensity I_{\perp}) with respect to the excitation polarization. Time-resolved anisotropy decay curves obtained from the streak camera measurements were essentially similar to those obtained from the TCSPC-based measurements. However, we resorted to the TCSPC-based method due to higher S/N of the traces from the latter.

(D) *Dynamic Quenching Experiments Using Acrylamide*. Aqueous acrylamide solution was added to the labeled protein samples in the concentration range 0–600 mM. Fluorescence lifetimes were measured immediately after the mixing. The bimolecular quenching constants (k_q) were estimated from the linear plot of τ_0/τ vs [Q], where τ_0 is the fluorescence lifetime in the absence of quencher and τ is the fluorescence lifetime in the presence of quencher at a concentration, [Q].

Data Analysis. (A) Generation of the Solvation Correlation Function. Fluorescence transient decays obtained from

the upconversion and the streak camera measurements at different wavelengths were plotted as shown in Figure 2. Various decay transient curves were produced from the streak images by setting the spectral window to a width of 15 nm. The multiexponential fitting analysis of each decay was carried out using a deconvolution method which takes into account the observed instrument response function. As the sensitivity of the detector may vary for different wavelength regions, it might cause some uncertainty in the intensity of the transient decay. Thus, the fluorescent transients at different wavelengths were corrected for the wavelength sensitivity of the detectors by using corrected steady-state emission spectra.

The multiexponential decays from the fits were normalized by the factors $F(\nu)/\sum a_i \tau_i$, where $F(\nu)$ is the steady-state fluorescence intensity, a_i are the preexponential factors, and τ_i are the decay times from the fits. Time-resolved emission spectra (TRES) were generated using a set of the corrected fluorescent transients taken at 15 nm intervals spanning the fluorescence spectrum. TRES were plotted at various times by taking the fluorescence intensity counts from the fluorescent decay transients at different wavelengths (Figure 3). TRES of the aggregated forms were generated only using the streak camera data. The main reason is that, in the aggregated forms, TDSS is very slow, and there was lack of data beyond lower side of 450 nm using the upconversion technique, and the peak of TRES was not obtained. In contrast, in the native and unfolded states, where the TDSS is much faster and within 400 fs, the peak of the TRES shifted to > 450 nm, and the peak of TRES was obtained for the upconversion technique. Thus, for the native and unfolded states, TRES was generated using both the upconversion and the streak camera data, whereas for the aggregated samples only the streak camera data could be used.

TDSS is related to a theoretical function, the so-called solvation correlation function, and the relaxation of the transient dipole around the fluorophores was monitored by following the

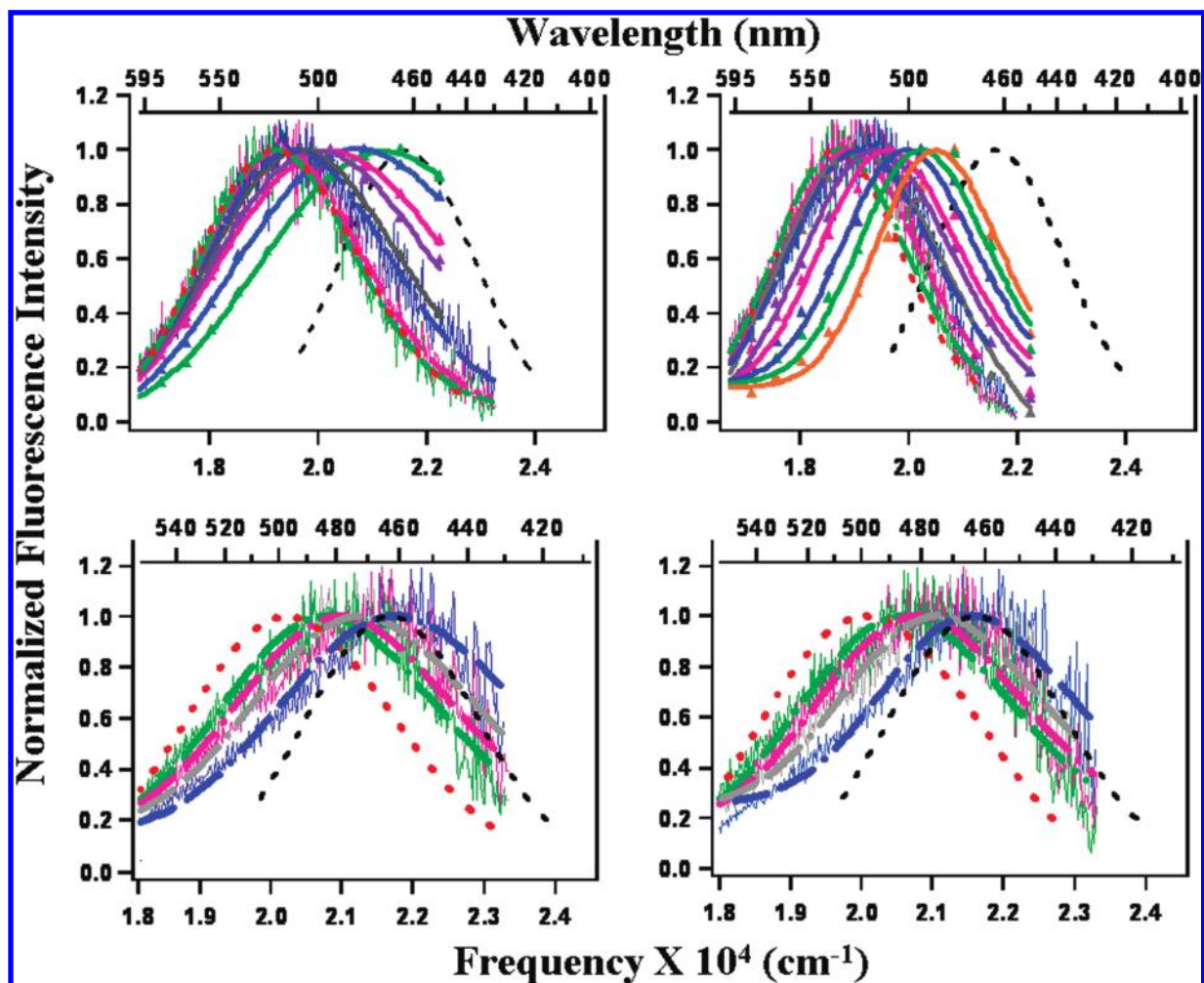


FIGURE 3: Time-resolved emission spectra (TRES) of the acrylodan-labeled Cys82 mutant. The two top panels show TRES of the native and unfolded forms at 0.4 ps (orange, Δ) (only in unfolded form), 1 ps (green, Δ), 2 ps (blue, Δ), 5 ps (pink, Δ), 10 ps (violet, Δ), and 50 ps (dark gray, Δ) obtained from fluorescence upconversion technique. The symbols Δ denote the actual values of fluorescence intensity, whereas the solid lines denote best fits of the TRES to the log normal function. The two panels also show TRES of the native and unfolded forms at 0.1 ns (blue, thin-solid line), 0.5 ns (pink, thin-solid line), and 0.8 ns (green, thin-solid line) generated using streak camera data. These thin-solid lines represent the actual data, whereas thick-dash lines represent best fits of the TRES to the log normal function. The lower two panels show TRES of the A form and the PF form at 0.1 ns (blue line), 0.3 ns (gray line), 0.5 ns (pink line), and 0.8 ns (green line) generated using streak camera data. These thin-solid lines represent the actual data, whereas thick-dash lines represent best fits of the TRES to the log normal function. Each panel shows a steady-state emission spectrum (red short-dash line) and a hypothetical spectrum at time $t = 0$ (black short-dash line) generated using the “full peak method” described earlier (20) (for detail, see Data Analysis), respectively.

decay of the solvation correlation function $C(t)$, which is defined as

$$C(t) = \frac{\nu(t) - \nu(\infty)}{\nu(0) - \nu(\infty)} \quad (1)$$

where $\nu(0)$, $\nu(t)$, and $\nu(\infty)$ represent the observed emission energies (frequencies) denote the peak of TRES at time zero, t , and infinity, respectively. Emission maxima $\nu(t)$ were determined by fitting these TRES to a log normal function. The value of $\nu(0)$ was estimated using PRODAN with the “full” method of Fee and Maroncelli (21). (We used PRODAN because it has the chemical structure of acrylodan attached to cysteine in protein (22).) The $\nu(0)$ was evaluated as 21581 cm^{-1} from the absorption spectrum of acrylodan-labeled Cys82 and absorption and fluorescence emission spectra of PRODAN in *n*-hexane. This $\nu(0)$ value was used for all of the mutant proteins because the absorption spectra of the dye-labeled mutant proteins are essentially the same. The value of $\nu(\infty)$ was taken as the frequency maximum at 25 ns, which overlaps with the steady-state emission spectrum for the respective sample. The former was obtained by streak camera data collected for 50 ns

time scale. The solvation correlation functions were generated, and these $C(t)$ curves were fitted using eq 2:

$$C(t) = \sum \alpha_i \exp(-t/\tau_i) \quad i = 2, 3 \quad (2)$$

where τ_i is the solvent relaxation time with amplitude α_i , such that $\sum \alpha_i = 1$.

(B) *Anisotropy Data Analysis.* The fluorescence anisotropy decay analysis was done in two steps. Initially, fluorescence intensity decay curves collected at the magic angle (54.7°) were analyzed by deconvoluting the observed decay with the IRF to obtain the intensity decay function represented as a sum of two or three exponentials as

$$I(t) = \gamma_i \exp(-t/\tau_i) \quad i = 2 \text{ or } 3 \quad (3)$$

where $I(t)$ is the fluorescence intensity at time t and γ_i is the amplitude associated with the fluorescence lifetime τ_i , such that $\sum \gamma_i = 1$.

These parameters were used as input for the anisotropy decay analysis. The time-resolved fluorescence anisotropy decays were

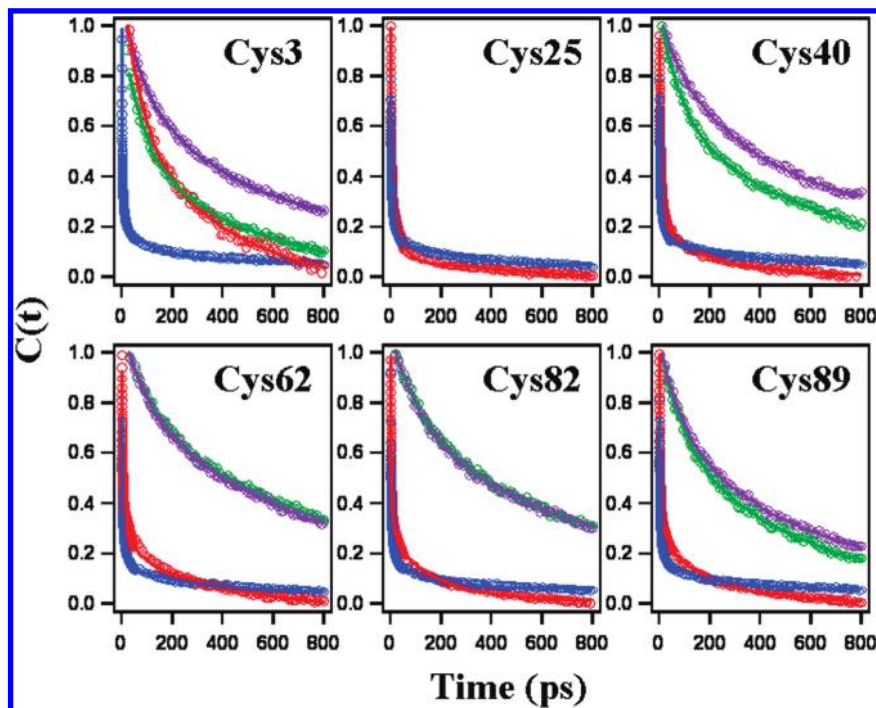


FIGURE 4: Decay kinetics of the solvation correlation function, $C(t)$. The decays of the solvation correlation function $C(t)$, of the acrylodan-labeled mutant proteins in the native state (red), the unfolded state (blue), the A form (green), and the PF form (violet), are shown. The symbols denote the actual values of $C(t)$, the solid lines denote the best fits to the sum of exponential decays (eq 2), and the parameters are listed in Table 1.

analyzed by globally fitting $I_{\parallel}(t)$ and $I_{\perp}(t)$ as

$$I_{\parallel}(t) = I(t)[1 + 2r(t)]/3 \quad (4)$$

$$I_{\perp}(t) = I(t)[1 - r(t)]/3 \quad (5)$$

where $I_{\parallel}(t)$ and $I_{\perp}(t)$ are the emission intensities collected at polarization directions parallel and perpendicular to the polarization of the excitation beam. $r(t)$ is the anisotropy decay function. The anisotropy decay was analyzed as a sum of exponential terms, as

$$r(t) = r_0 \sum \beta_j \exp(-t/\phi_j) \quad j = 2, 3 \quad (6)$$

where r_0 is the limiting anisotropy in the absence of rotational diffusion and ϕ_j are the rotational correlation times with amplitude β_j , such that $\sum \beta_j = 1$. This model assumes a population having uniform fluorescence dynamics properties with each molecule associated with both of the correlation times. The goodness of fits was assessed from the values of the reduced chi-square (1.0–1.2) and randomness of residuals.

While analyzing the anisotropy decay traces by using eqs 3–6, the parameters associated with the fluorescence intensity decay were kept (with $\sim 20\%$ window) at the values obtained from the analysis of fluorescence intensity decays collected at the magic angle with respect to the excitation polarization. Furthermore, the initial anisotropy, r_0 , was also estimated from an independent experiment in which the decay of the fluorescence anisotropy of the free acrylodan in 70% glycerol was measured and kept fixed at this value (0.33 ± 0.005) while analyzing the anisotropy decay kinetics of the samples. Thus, in the analysis of the anisotropy decay curves, the number of free parameters gets reduced substantially, increasing the reliability of the estimates of the parameters associated with the anisotropy decay. This procedure guides the software toward the global minimum. This procedure was in fact benchmarked against samples which show a single

lifetime as well as a single rotational correlation time (data not shown). For such samples we recovered the same parameters either by fixing the lifetime value (with or without 20% window) or by keeping “all” of the parameters floating.

The errors associated with the parameters extracted from anisotropy decay curves were estimated in the following ways: (i) by repeated analysis of the traces with different sets of initial parameters, (ii) by analysis of several different decay curves, and (iii) by fixing one of the parameters at various values and floating the other parameters and critically evaluating both the chi-square values and the randomness of the residuals.

We ensured that the TCSPC method with a time resolution of 40 ps does not miss any faster rotational correlation times by the observation that the shortest correlation time ($\phi_1 \sim 60\text{--}400$ ps) gives the value of the zero-time anisotropy (r_0) as observed either for the probe alone or for the labeled protein in glycerol–water mixtures where all of the rotational dynamics are highly damped. These observations indicate that we do capture rotational dynamics completely without missing any ultrafast component.

(C) *Dynamic Quenching Constant (k_q)*. The bimolecular quenching constant (k_q) was estimated from the linear plot of τ_0/τ_m vs $[Q]$:

$$\frac{\tau_0}{\tau_m} = 1 + k_q \tau_0 [Q] \quad (7)$$

where τ_0 is the fluorescence lifetime in the absence of quencher and τ_m is the mean fluorescence lifetime and defined as $\tau_m = \sum \tau_i \gamma_i$ (where $i = 2, 3$) and γ_i is the amplitude associated with the fluorescence lifetime τ_i in the presence of quencher at a concentration $[Q]$. The slope of the Stern–Volmer plot, i.e., the Stern–Volmer constant, K_{sv} is equal to $k_q \tau_0$. Fluorescence lifetime τ_i and its amplitude γ were obtained by deconvoluting the intensity decay collected at magic angle with the IRF and represented as a sum of two or three exponentials as described by eq 3.

Table 1: Solvent Relaxation Times and Their Amplitudes Obtained by Analyzing $C(t)$ Curves Using the Multiexponential Decay eq 2 for the Different Conformational States of All Six Mutant Proteins Labeled with the Acrylodan Probe^a

protein	τ_1 , ps (α_1)	τ_2 , ps (α_2)	τ_3 , ps (α_3)	τ_s , ps	missing component
Cys3 native		29.2(0.73)	325(0.27)	109.1	0
Cys25 native	1.22(0.72)	19.4(0.18)	155(0.10)	19.87	0
Cys40 native	1.67(0.48)	9.71(0.34)	160(0.18)	32.4	0
Cys62 native	1.21(0.61)	12.4(0.20)	232(0.19)	47.3	0
Cys82 native	1.51(0.63)	13.4(0.17)	190(0.20)	42.3	0
Cys89 native	1.90(0.53)	23.1(0.31)	220(0.16)	43.2	0
Cys3 unfolded	0.53(0.61)	7.21(0.27)	150(0.12)	20.0	0
Cys25 unfolded	1.33(0.50)	11.1(0.32)	160(0.18)	28.4	0.30
Cys40 unfolded	1.32(0.51)	10.9(0.34)	151(0.15)	28.4	0.31
Cys62 unfolded	1.35(0.53)	10.3(0.31)	129(0.16)	23.6	0.29
Cys82 unfolded	0.56(0.53)	7.44(0.34)	160(0.13)	24.1	0.16
Cys89 unfolded	1.51(0.54)	9.20(0.30)	149(0.16)	27.3	0.30
Cys3 A form		45.2(0.47)	372(0.53)	218.4	0
Cys40 A form		75.2(0.48)	490(0.52)	290.9	0
Cys62 A form		75.4(0.41)	578(0.59)	371.9	0
Cys82 A form		89.0(0.42)	575(0.58)	370.9	0
Cys89 A form		84.0(0.48)	540(0.52)	322.7	0
Cys3 PF		55.0(0.40)	305(0.68)	229.4	0
Cys40 PF		85.4(0.47)	605(0.53)	360.8	0
Cys62 PF		79.5(0.47)	612(0.53)	361.7	0
Cys82 PF		72.0(0.40)	561(0.60)	365.4	0
Cys89 PF		55.0(0.43)	545(0.57)	334.3	0

^aFor the unfolded mutants the missing component is not considered while calculating τ_s . Mean solvent relaxation time, τ_s , is defined as $\tau_s = \tau_1\alpha_1 + \tau_2\alpha_2 + \tau_3\alpha_3$ (where $\alpha_1 + \alpha_2 + \alpha_3 = 1$). Errors are not mentioned explicitly in order to improve clarity. Errors associated with each measurement are $\sim 10\%$.

RESULTS

Femtosecond-Resolved Fluorescence Transients and Solvation Dynamics. Figure 2 shows the femtosecond-resolved fluorescence transients of acrylodan coupled to C82 of the single cysteine mutant form Cys82, collected at four typical gated wavelengths, i.e., 450, 480, 525, and 570 nm, obtained using either fluorescence upconversion or a streak camera for detection. The fluorescence upconversion system (time resolution ~ 200 fs) was used for the time window 200 fs to 50 ps, and the streak camera (time resolution ~ 20 ps) was used for the time window 50 ps to 1 ns. The results show ultrafast decays on the blue side of the spectrum and corresponding rises in the red edge, features that form a signature of TDSS. The fluorescence transients showed similar patterns for the other five mutant proteins, in all four conformational states. TDSS is generally interpreted as due to solvent relaxation around the fluorophore (23, 24) (see Discussion).

All of the fluorescence transients could be fitted to the sum of two or three exponentials for both the rising and decaying regions of the curves (see Supporting Information Table S1 for the fitting parameters). The time constants ranged from 300 fs to 10 ns. Smooth curves generated by fits to the fluorescence transients were used to construct time-resolved emission spectra (TRES) (see Data Analysis section in Methods). Typical TRES for the Cys82 mutant protein are shown in Figure 3 Emission maxima ν_r were determined by fitting these TRES to a log normal function. The time zero peak position was estimated by the “full” method of Fee and Maroncelli described earlier (21). This method is based on a simple model of the inhomogeneous broadening of bands in polar solvents. The excitation and emission spectra in a nonpolar medium like *n*-hexane are used as references to calculate the time zero spectrum. Solvation correlation functions

$C(t)$ estimated from the TDSS of the TRES traces are shown in Figure 4. The time constants obtained from fitting these $C(t)$ traces to a sum of exponentials are summarized in Table 1. The missing amplitude represents processes too fast to be observed with our 200 fs time resolution.

A recent work on an analogue of acrylodan has indicated a possible complication while interpreting TDSS arising from a locally excited state transforming into a charge transfer state (25). Two bands seen in their emission spectra were assigned to the two states, and the kinetics of TDSS was different for different emission bands (25). Such a situation is unlikely to be present in our experiments, as our emission spectra do not show any indication of multiple emission bands.

Multiple time scales observed in TDSS (Table 1) have indeed been observed in several systems (26–29). Although these time constants have been hypothesized to arise from various dynamic processes, such as moderately damped water molecules and dynamics of water in the first solvation shell, there is no universal acceptance of such proposals (7, 30) (see ref 9 for an alternate view).

While all of the three time constants observed in the native proteins show position dependence, the behavior seen for the Cys3 protein is remarkably different. The buried nature of C3 (see later) could explain the relatively slow decay of $C(t)$, compared to the decays seen at other locations (Table 2). It would be interesting to see whether this variation correlates with the structure and solvent accessibility (see later). Unlike the native protein, the unfolded protein shows much less position dependence of the solvation dynamics and a significant level (0.16–0.31) of missing amplitude. The enhanced solvent exposure in the U state is expected to accelerate solvation dynamics.

The situation in the case of the A and PF forms is distinct from either the N or U forms. First, TRES could not be constructed

Table 2: Rotational Correlation Times and Their Amplitudes Obtained by Analyzing Anisotropy Decay Curves Using the Multiexponential Decay eqs 3–6 for the Different Conformational States of All Six Mutant Proteins Labeled with the Acrylodan Probe^a

protein	$\phi_1\beta_1$ (local), ns	$\phi_2\beta_2$ (segmental), ns	$\phi_3\beta_3$ (global), ns	ϕ_{mean} , ns	$\phi_{\text{seg+local}}$, ns
Cys3 native	0.18 (0.12)	2.55 (0.29)	4.9 (0.59)	3.65	1.86
Cys25 native	0.07 (0.11)		4.8 (0.89)	4.37	0.07
Cys40 native	0.08 (0.17)		4.8 (0.83)	4.08	0.08
Cys62 native	0.40 (0.27)		4.9 (0.73)	3.68	0.40
Cys82 native	0.34 (0.11)		4.8 (0.89)	4.39	0.34
Cys89 native	0.12 (0.28)	0.72 (0.19)	5.1 (0.53)	2.77	0.36
Cys3 unfolded	0.33 (0.54)		1.75 (0.46)	0.98	
Cys25 unfolded	0.42 (0.52)		3.80 (0.48)	2.04	
Cys40 unfolded	0.39 (0.54)		1.84 (0.46)	1.05	
Cys62 unfolded	0.35 (0.52)		2.25 (0.48)	1.26	
Cys82 unfolded	0.36 (0.54)		2.90 (0.46)	1.53	
Cys89 unfolded	0.39 (0.75)		2.30 (0.25)	0.87	
Cys3 A form	0.12 (0.31)		76 (0.69)	53.85	0.12
Cys40 A form	0.09 (0.33)	2.30 (0.12)	80 (0.56)	43.98	0.68
Cys62 A form	0.09 (0.22)	3.40 (0.21)	78 (0.57)	45.19	1.71
Cys82 A form	0.06 (0.16)	2.5 (0.25)	79 (0.59)	46.65	1.55
Cys89 A form	0.08 (0.24)	2.1 (0.21)	81 (0.55)	43.36	1.02
Cys3 PF	0.09 (0.28)		> 100 (0.72)	360	0.09
Cys40 PF	0.20 (0.21)	2.5 (0.15)	> 100 (0.64)	320	1.16
Cys62 PF	0.16 (0.15)	2.1 (0.19)	> 100 (0.66)	330	1.24
Cys82 PF	0.13 (0.15)	2.5 (0.19)	> 100 (0.66)	330	1.45
Cys89 PF	0.12 (0.2)	2.1 (0.18)	> 100 (0.62)	310	1.05

^a $\phi_{\text{mean}} = \sum \phi_i \beta_i$ ($i = 3$) (where $\beta_1 + \beta_2 + \beta_3 = 1$) and $\phi_{\text{seg+local}} = \phi_1 \beta_1 + \phi_2 \beta_2$ (where $\beta_1 + \beta_2 = 1$). Also, ϕ_{mean} was calculated using the value of $\phi_3 = 4.9, 78,$ and 500 ns for the native state, the A form, and the PF form, respectively. Errors are not mentioned explicitly in order to improve clarity. Errors associated with each measurement are $\sim 20\%$ for ϕ_1 and β_1 and $\sim 10\%$ for others.

from the upconversion data (see Data Analysis section), and hence, the earliest time point was 20 ps. The following observations are worth noting: (i) The two observable time constants are significantly longer when compared to the N and U forms. (ii) The ~ 1 ps time constant which is the predominant component for the N and U forms cannot be estimated. (iii) The mean solvation time is very similar for all of the positions except for the Cys3 protein which has significantly lower values for both the A and PF forms.

Internal Protein Dynamics Measured by Fluorescence Anisotropy Decay Kinetics. The motional dynamics of acrylodan coupled to cysteine at various locations was studied using time-resolved fluorescence anisotropy decay. Typical time-resolved fluorescence traces are shown for Cys82 in Figure 5. For different mutant protein samples, the decay kinetics could be fitted to the sum of two or three exponentials. Table 2 gives the results of analysis based on eqs 3–6 (see Data Analysis section).

All of the native proteins, except Cys3 and Cys89, are associated with two correlation times, one 4.9 ns, corresponding to the global dynamics (31, 32), and another in the range of 0.07–0.40 ns, corresponding to the local motion of the fluorophore. Position-dependent variation in the value and amplitude of the correlation time corresponding to the local motion is expected for a structured protein (see later). Similarly, the observation of an intermediate correlation time which could be ascribed to segmental dynamics can also be related to the structures and dynamics of N- and C-terminal regions of the native protein.

Motional dynamics of the fluorophore in the U state is significantly faster than in the N state, as expected. While the faster component could again be assigned to the local motion of the probe, the longer component could have contributions from

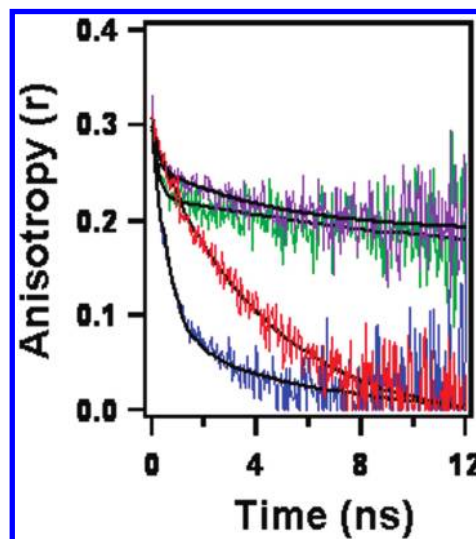


FIGURE 5: Various states of mutant protein show different dynamics. Time-resolved fluorescence anisotropy decay kinetics of the acrylodan-labeled Cys82 mutant protein in the native state (red), the unfolded state (blue), the A form (green), and the PF form (violet). The smooth black lines are the fits to eqs 3–6, and the parameters are listed in Table 2.

both the global tumbling dynamics of the polypeptide and the segmental motion (32).

The A form and the PF form show motional dynamics very similar to each other except for the longest correlation time. The longer value (> 100 ns) for the PF form when compared to that of the A form (~ 80 ns) is a reflection of the larger size of the former. The other two correlation times show position dependence in their values and amplitudes, reflecting, once again, structural details (11).

Table 3: Acrylamide Quenching of IAEDANS Attached to Protein: Stern–Volmer Constants (K_{sv}) and Bimolecular Quenching Rate Constant (k_q) Obtained by Analyzing Stern–Volmer Plots Using eq 7 for the Different Conformational States of All Six Mutant Proteins^a

mutant	native		unfolded		A form		PF	
	K_{sv} (M^{-1})	$k_q \times 10^8$ ($M^{-1} s^{-1}$)	K_{sv} (M^{-1})	$k_q \times 10^8$ ($M^{-1} s^{-1}$)	K_{sv} (M^{-1})	$k_q \times 10^8$ ($M^{-1} s^{-1}$)	K_{sv} (M^{-1})	$k_q \times 10^8$ ($M^{-1} s^{-1}$)
Cys3	2.90	2.23	6.92	6.35	3.43	3.01	3.98	3.09
Cys25	7.69	7.76	7.48	8.87				
Cys40	6.45	6.23	7.12	6.65	1.43	0.86	0.88	0.57
Cys62	6.81	6.61	7.72	7.72	1.07	0.52	0.93	0.78
Cys82	6.25	6.01	6.98	7.01	1.04	0.51	0.88	0.55
Cys89	8.21	8.11	9.05	8.89	1.64	1.01	0.86	0.73

^aErrors associated with each measurement are < 10%.

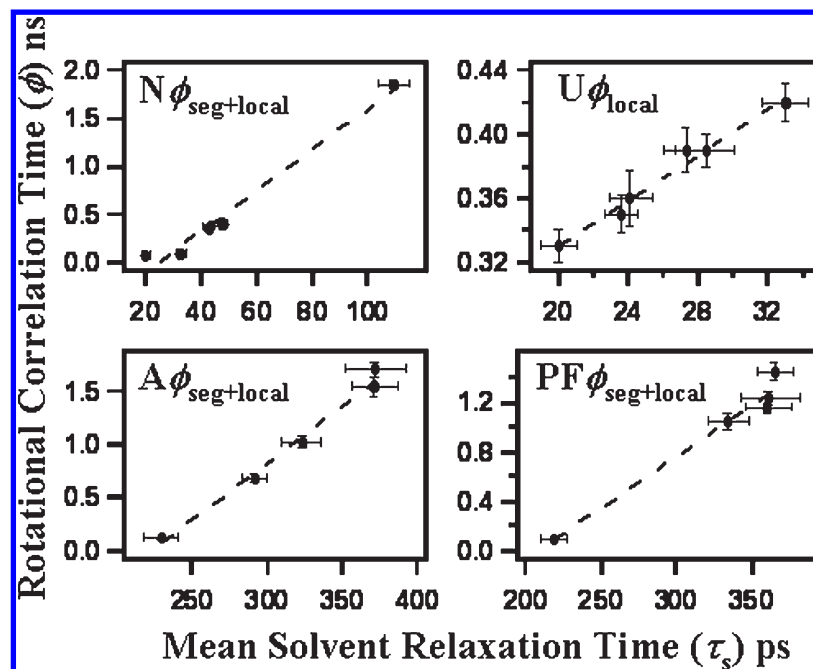


FIGURE 6: Correlation of solvation dynamics and internal dynamics of protein. Each panel shows the correlation of the mean solvent relaxation time (τ_s) with segmental (ϕ_2) + local motion (ϕ_1) of the acrylodan-labeled mutant proteins in the native (N), unfolded (U), A form (A) and PF forms (PF). Mean solvent relaxation time, τ_s , is defined as $\tau_s = \tau_1\alpha_1 + \tau_2\alpha_2 + \tau_3\alpha_3$ (where $\alpha_1 + \alpha_2 + \alpha_3 = 1$). Internal dynamics of protein is defined as $\phi_1\beta_1 + \phi_2\beta_2 = \phi_{seg+local}$ (where $\beta_1 + \beta_2 = 1$), where the values for $\phi_{seg+local}$ for the respective mutant proteins are taken from Table 2. The \bullet symbols denote the actual values, and the dashed lines denote the best linear fits to the data. The error bars represent the standard deviations obtained from three separate sets of experiments.

Solvent Exposure Estimation by Acrylamide Quenching. The main aim set out in this work was to explore the correlation between solvation dynamics probed by TDSS and motional dynamics probed by fluorescence anisotropy decay kinetics. In this context, an assessment of the level of solvent exposure adds another relevant dimension to this exploration. An estimation of solvent accessibility could also resolve the issue whether the slower solvation dynamics of the aggregated form is due to the fluorophore being buried or is due to extra rigidification of surface water in the fibrils. Dynamic quenching of fluorescence is an effective way of estimating solvent accessibility of side chains in proteins (33). Since we could not find an appropriate quencher for acrylodan, we used 1,5-IAEDANS (5-(((2-iodoacetyl)-amino)ethyl)amino)naphthalene-1-sulfonic acid) as the fluorescence probe for quenching studies (11). Supporting Information Figure S1 shows typical Stern–Volmer plots for quenching by acrylamide. Bimolecular quenching constants, k_q , estimated from these plots are given in Table 3.

Several interesting observations are worth noting: (i) The values of k_q for the native proteins are slightly lower than those

for the unfolded proteins, except for Cys3 where it is significantly reduced in the native state, indicating the buried nature of C3 in the native protein. (ii) Although the extent of variation in the value of k_q is less for the U state than for the N state, the pattern of variation is somewhat preserved for the unfolded protein. (iii) k_q shows a significant reduction in value (except in the case of Cys3) for both the A and PF forms when compared to either the N or the U form, indicating a significant reduction in the level of solvent accessibility. (iv) The remarkably high values of k_q for Cys3 in the A and PF forms, when compared to the values at the other locations, indicate the noninvolvement of the N-terminal region in the rigid core of the fibrils (15, 17).

Correlation between TDSS and Internal Protein Dynamics. Since the kinetics of solvent relaxation as well as of fluorescence anisotropy decay are multiexponential, exploration of the correlation between solvent relaxation and motional dynamics is expected to be selective among the various decay components. Identification of the various decay components would make such the correlation physically meaningful. In the case of solvent relaxation (TDSS), assignment of the various

components to a specific process is not unique, and hence, we use the mean solvent relaxation time, which is a weighted average of the various observed components. In contrast, identification of the decay components associated with fluorescence anisotropy is less controversial. The short correlation time represents the local internal dynamics of the probe, and the middle component is assigned to segmental dynamics of the region of the polypeptide to which the probe is attached. Thus, the flexibility of the probe would be reflected in both the local and segmental dynamics extracted from anisotropy decay kinetics.

Figure 6 shows the plots of a combination of fluorescence anisotropy decay time constants (see the legend to Figure 6 for details of merging of time constants of $\phi_1 + \phi_2$) versus the mean solvent relaxation time (τ_s). The results indicate a linear correlation between τ_s and a combination of local (ϕ_1) and segmental (ϕ_2) motion in the N, A, and PF forms. In the case of the U form, the best linear correlation is found between τ_s and the time constant associated with the local motion (ϕ_1). An interesting observation is the absence of correlation when the global tumbling dynamics is also included (Supporting Information Figure S2). The global dynamics is not expected to have any correlation to the site-specific solvation dynamics measured around the fluorophore using TDSS, unlike the other two components which are related to the flexibility of the group with respect to the protein matrix.

In the correlation plots shown in Figure 6, the mean solvation time, τ_s , is used in all of the panels. τ_s is a weighted mean of all the solvation time constants (Table 1) except the unresolved missing component. It is interesting to note that no significant correlation was seen when individual components of solvation kinetics are plotted against the time constant arising from internal protein dynamics (data not shown).

Correlation between Solvation Dynamics and Solvent Accessibility. As noted earlier, the bimolecular quenching constant k_q which provides a reliable measure of the solvent accessibility showed a dramatic variation depending on both the position of the fluorophore in the sequence and the structural form of the protein. Does k_q correlate with the solvation time τ_s ? Figure 7 provides the answer to this question. The mean solvation time is linearly dependent on the inverse of k_q (Figure 7), indicating significant correlation between these two observables.

DISCUSSION

The central importance of dynamics in protein function and the intimate connection with water demands that we seek in-depth information on various dynamic aspects of the protein–water system treated as a single entity. A large variety of experimental methods which are being employed to study protein dynamics address various dynamic modes occurring in the time scales of femtoseconds to microseconds (12, 34–36).

TDSS of either the intrinsic fluorophore tryptophan or of site-specifically labeled extrinsic fluorophores attached to a protein has been the most popular technique to study the solvation dynamics and quantify the rigidity of the solvation shell and local protein flexibility at protein–water interfaces (6, 23). A fundamental difficulty in the interpretation of TDSS is that it can arise from either or both of the following two processes: (i) reorientation of the solvent around the probe and (ii) conformational dynamics of the probe itself (37).

According to the popular model of interpreting TDSS, the fast component (< 1 ps) is assigned to the dielectric relaxation of bulk

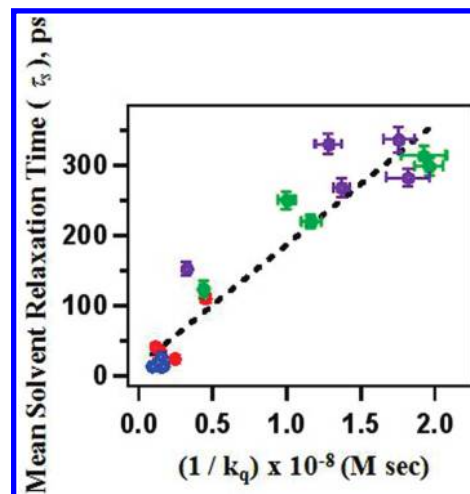


FIGURE 7: Correlation of solvation dynamics and solvent accessibility of different residues. The correlation of the mean solvent relaxation time (τ_s) with inverse of the bimolecular quenching constants (k_q) estimated from the linear Stern–Volmer plot (see Supporting Information for details) for different mutant proteins in the native state (red \circ), the unfolded state (blue \circ), the A form (green \circ), and the PF form (violet \circ). Mean solvent relaxation time, τ_s , is defined as $\tau_s = \tau_1\alpha_1 + \tau_2\alpha_2 + \tau_3\alpha_3$ (where $\alpha_1 + \alpha_2 + \alpha_3 = 1$). The \bullet symbols denote the actual values, and the dashed lines denote the best linear fit to the data. The error bars represent the standard deviations obtained from three separate sets of experiments.

water, and the slower (> 10 ps) components are assigned to the hydration layer commonly referred by some researchers as “biological water” (29, 38, 39). While the solvation dynamics of free fluorophores are in the subpicosecond range (40), the time scale becomes reduced by 2–3 orders of magnitude for a fluorophore attached to a protein (6, 41, 42). The assignment of this slow process to a rigid hydration layer implies a very long residence time (~100 ps or longer) of bound water. This model has, however, been questioned by Halle and co-workers based on their ^{17}O NMR relaxation measurements which appear to show that ~90% of the interfacial water molecules have residence times which are only 2-fold longer compared to those of bulk water and which are similar to those in the hydration shells of small organic solutes (9, 37, 43).

An alternative way of estimating the level of flexibility is to monitor time-resolved fluorescence anisotropy decay (11). Is there a correlation between these two classes of observations, viz., one in which the immediate environment around the probe is monitored and the other in which the motion of the probe is directly monitored? Establishing this correlation will have several implications: (i) direct coupling between the motional dynamics of proteins and solvent fluctuations would be consistent with the idea that the protein dynamics are slaved to the solvent dynamics (8), and (ii) measurement of one could be used to predict the other.

The linear correlation observed between the “solvation dynamics” around the protein-linked fluorophore and the motional dynamics of the fluorophore (Figure 6) clearly establishes the connection between these two dynamic modes. Although similar correlations have been suggested in earlier studies (6), the present work derives its strength from the large number of samples, which bring out the significant level of variation in the kinetics of TDSS and the motional dynamics of the probe, thus enabling the exploration of the correlation between these two dynamic modes.

The question whether the dynamic process monitored by the TDSS can be identified as the conformational dynamics of the

probe rather than solvation dynamics around the probe has been addressed in earlier studies. An early observation in this respect was the suggestion of solvent dipole-driven rapid rotation of coumarin 153 (44). Following absorption, the misaligned solvent dipole field produces an instantaneous torque on the solute dipole. This causes a forced rotation of the solute, and this forced rotation could be faster than diffusive motion and be observed as a rapid component in fluorescence anisotropy decay kinetics (44). It is interesting to note that this model does not support the slaving model wherein the motion of the solute is driven by the fluctuations arising in the solvent (8).

An assignment of the observed kinetics of TDSS to protein dynamics could imply similar time scales for both of the processes. The origin of TDSS lies in dielectric relaxation of solvent molecules for which the orientation autocorrelation function is given by the Legendre polynomial of order 1:

$$\langle P_1[\cos \theta(t)] \rangle = \cos \theta(t)$$

where $\theta(t)$ is the time-dependent orientation of the solute dipole with respect to the solvent dipole field. In contrast, the fluorescence anisotropy decay ($r(t)$) experiment measures the second-order Legendre polynomial orientation autocorrelation function, P_2

$$r(t) = r_0 \langle P_2[\cos \theta(t)] \rangle = r_0 (3 \cos^2 \theta(t) - 1) / 2$$

It can be shown that the exponential time constant associated with the decay of $\langle P_2[\cos \theta(t)] \rangle$ is 3-fold faster than the decay of $\langle P_1[\cos \theta(t)] \rangle$. This was indeed observed in the case of coumarin 153 (44). Such a comparison is not straightforward in the present work due to the presence of several time constants for both the TDSS and fluorescence anisotropy decay kinetics (Tables 1 and 2). It is, however, noted that the longest solvation time τ_3 (usually assigned to biological water or the hydration layer) and the shortest rotational correlation time ϕ_1 (usually assigned for local motion of the probe attached to the protein side chain) are in a comparable range of 100–600 ps (Tables 1 and 2). We do not find any significant correlation between these two individual time constants (τ_3 and ϕ_1) (Supporting Information Figure S3). This lack of correlation between τ_3 and ϕ_1 and the observed correlation when a combination of time constants is used (Figure 6) suggests that both the solvation and the motional dynamics are contained in more than one time constant in each process.

While the linear correlation observed between the mean solvation time and a combination of local and segmental dynamics extracted from time-domain fluorescence anisotropy (Figure 6) is quite interesting and notable, equally important is the observation of an absence of correlation when either only one of the dynamic modes (either local or segmental or global) (data not shown) or a combination of *all* three modes is taken into account (Supporting Information Figure S2). This suggests that (i) the solvation dynamics estimated through TDSS is essentially coupled to the local and segmental modes of the protein dynamics and (ii) the global tumbling dynamics of proteins is not coupled to solvation dynamics.

It was possible to express the linear correlation observed between the solvation dynamics and the protein dynamics as a scaling law of the form $\phi_p = x + y\tau_s$, where ϕ_p is a combination of local and segmental dynamics and y is the scaling factor. The “offset” value x could have its origin in the choice of the components of either the solvation dynamics or the motional dynamics included in the correlation plots. The value of y is 21.4 ± 1.6 ,

7.2 ± 0.5 , 10.8 ± 0.7 , and 8.3 ± 0.8 for the N, U, A, and PF forms, respectively. The value of x is $-5.3 (\pm 0.9) \times 10^{-10}$, $1.9 (\pm 0.1) \times 10^{-10}$, $-23.9 (\pm 2.2) \times 10^{-10}$, and $-17.3 (\pm 2.8) \times 10^{-10}$ s for the N, U, A, and PF forms, respectively.

The linear correlation between the dynamic modes observed in this work (Figure 6) is on the lines expected from the “slaving” model of Frauenfelder and co-workers (8, 10, 45). According to this model, conformational motions in proteins are slaved to the solvent fluctuations in the hydration shell and in the bulk solvent. Their recent measurements on solvent fluctuations using dielectric spectroscopy and on protein internal fluctuations with the Mossbauer effect and neutron scattering support their model (8). It is important to realize that although the two dynamic processes, viz., solvation monitored by TDSS and conformational dynamics detected by fluorescence anisotropy decay kinetics, are coupled to each other, their time scales are not identical. This is observed both in the present work and in the recent work of Frauenfelder and co-workers (8). As mentioned before, if the same dynamic process is being observed through the two techniques, it is expected that the scaling factor y (see above) would be $1/3$ as seen in the case of coumarin 153 (44). The value of y observed in the experiments reported here is in the range of 7–21, thus ruling out this model, which is similar to that proposed by Halle and co-workers (9). Another consequence of the observed TDSS being not the direct result of conformational dynamics of the protein-linked fluorophore is the following: The observed TDSS is due to slow solvation dynamics and the retardation of this dynamics compared to that of bulk water (< 1 ps) is due to the special nature of “biological water” which is partially immobilized at the protein–water interface (38).

A more plausible model for explaining the observed correlation between the TDSS and the motional dynamics monitored by fluorescence anisotropy decay kinetics (Figure 6) is one in which the two different techniques score two different dynamic modes which are coupled to each other. Fluctuations in bulk water and in the hydration layer, occurring on the time scale of 1–100 ps, could dictate the motional dynamics of protein side chains and segments, which occur on the relatively longer time scales of 100 ps to 2 ns in spite of the difference in the time scales of the two processes. The significantly longer time scale associated with the motional dynamics when compared to that of the solvation process can be viewed as due to a large number of elementary steps needed for effective control of the conformational dynamics of proteins by fluctuations arising in bulk water and in the hydration layer. Motion of protein side chains cannot occur following a single step motion of a solvent molecule but could occur as a consequence of several such movements of the solvent molecules surrounding side chains. This is similar to the proposal by Frauenfelder and co-workers (46, 47). According to their model, the value of y (see above) would represent the number of elementary steps involved in the coupling. The consequences of this interpretation are that it becomes possible to predict the time scale of one dynamic mode from knowledge of the other mode and that the value of y can be used to shed light on the actual mechanism of coupling.

It is interesting to note that studies of time-resolved anisotropy on the protein-bounded probe aladan did not reveal any significant reorientation of the probe in the time scale of the solvation process, thus excluding the movement of the probe itself as the source of the solvation dynamics (48). This conclusion is similar to that derived from the present studies. A contrasting scenario is, however, derived from molecular dynamics simulations. Halle

and Nilsson concluded, based on molecular dynamics simulations, that the slow component emerging in TDSS arises from slow conformational fluctuations in proteins and not from slow protein hydration dynamics (9, 37). The molecular dynamics simulations by Golosov and Karplus showed, however, that a simple assignment of the various components of TDSS, such as the short time scale component to solvent relaxation and the longer component to protein dynamics, cannot always be made (5). The identification of the slow component observed in TDSS as due to either slow hydration dynamics or protein motion varied from one location to another (5). The current study is timely in the context of ongoing efforts to resolve the issue regarding the coupling between the various dynamic modes in protein–water systems.

Site Specificity of Solvation Dynamics in Various Protein States. One of the accrued benefits from the present work is the information on the site specificity of solvation dynamics in a protein in its various states such as the N, U, A, and PF forms. The present work provides information on a number of sites along the sequence and, hence, would be of use in inferring the dependence of solvation dynamics on the local environment. For example, the significantly slower solvation dynamics observed for Cys3 and faster dynamics for Cys25 in their native states (Table 1) correlate well with the level of solvent exposure as estimated from fluorescence quenching (Table 3 and Figure 7). An increase in the solvation time constant parallels a decrease in the value of the quenching constant, k_q (Tables 1 and 3). A similar correlation between the solvation kinetics and solvent exposure has been shown by molecular dynamics simulations in a 36-residue globular protein, HP-36 (49).

A significant reduction in the level of solvent exposure (smaller value of k_q), seen for the A forms as well as the PF forms, points to the buried nature of the probe in these structural forms, resulting the slower solvation dynamics. Buried probes displaying slower solvation dynamics when compared to surface-exposed probes have been seen earlier both experimentally (50) and in MD simulations (49). Furthermore, for any buried probe, the observed TDSS is likely to have a major contribution from the dynamics of nearby dipoles of the surrounding protein matrix apart from the dynamics of the solvent. Thus, the TDSS for such probes might be an indicator of the relative flexibility of the surrounding matrix with respect to the probe.

ACKNOWLEDGMENT

We thank Prof. N. Periasamy for providing the software for the analysis of time-resolved fluorescence data. We also thank Dr. Sudip Kumar Mondal for help in calculating the $\nu(0)$ value in the analysis of TDSS.

SUPPORTING INFORMATION AVAILABLE

Table S1 and Figures S1–S3 providing a description of experiments that support the main conclusions. This material is available free of charge via the Internet at <http://pubs.acs.org>.

REFERENCES

- Berendsen, H. J., and Hayward, S. (2000) Collective protein dynamics in relation to function. *Curr. Opin. Struct. Biol.* 10, 165–169.
- Henzler-Wildman, K., and Kern, D. (2007) Dynamic personalities of proteins. *Nature* 450, 964–972.
- Smock, R. G., and Gierasch, L. M. (2009) Sending signals dynamically. *Science* 324, 198–203.
- Longworth, L. G. (1954) Temperature dependence of diffusion in aqueous solutions. *J. Phys. Chem.* 58, 770–773.
- Golosov, A. A., and Karplus, M. (2007) Probing polar solvation dynamics in proteins: a molecular dynamics simulation analysis. *J. Phys. Chem. B* 111, 1482–1490.
- Zhang, L., Wang, L., Kao, Y. T., Qiu, W., Yang, Y., Okobiah, O., and Zhong, D. (2007) Mapping hydration dynamics around a protein surface. *Proc. Natl. Acad. Sci. U.S.A.* 104, 18461–18466.
- Bhattacharyya, K. (2008) Nature of biological water: a femtosecond study. *Chem. Commun. (Cambridge)*, 2848–2857.
- Frauenfelder, H., Chen, G., Berendzen, J., Fenimore, P. W., Jansson, H., McMahon, B. H., Strope, I. R., Swenson, J., and Young, R. D. (2009) A unified model of protein dynamics. *Proc. Natl. Acad. Sci. U.S.A.* 106, 5129–5134.
- Halle, B., and Nilsson, L. (2009) Does the dynamic Stokes shift report on slow protein hydration dynamics? *J. Phys. Chem. B* 113, 8210–8213.
- Fenimore, P. W., Frauenfelder, H., McMahon, B. H., and Young, R. D. (2004) Bulk-solvent and hydration-shell fluctuations, similar to alpha- and beta-fluctuations in glasses, control protein motions and functions. *Proc. Natl. Acad. Sci. U.S.A.* 101, 14408–14413.
- Mukhopadhyay, S., Nayak, P. K., Udgaonkar, J. B., and Krishnamoorthy, G. (2006) Characterization of the formation of amyloid protofibrils from barstar by mapping residue-specific fluorescence dynamics. *J. Mol. Biol.* 358, 935–942.
- Saxena, A. M., Udgaonkar, J. B., and Krishnamoorthy, G. (2006) Characterization of intra-molecular distances and site-specific dynamics in chemically unfolded barstar: evidence for denaturant-dependent non-random structure. *J. Mol. Biol.* 359, 174–189.
- Jha, S. K., and Udgaonkar, J. B. (2007) Exploring the cooperativity of the fast folding reaction of a small protein using pulsed thiol labeling and mass spectrometry. *J. Biol. Chem.* 282, 37479–37491.
- Swaminathan, R., Krishnamoorthy, G., and Periasamy, N. (1994) Similarity of fluorescence lifetime distributions for single tryptophan proteins in the random coil state. *Biophys. J.* 67, 2013–2023.
- Juneja, J., Bhavesh, N. S., Udgaonkar, J. B., and Hosur, R. V. (2002) NMR identification and characterization of the flexible regions in the 160 kDa molten globule-like aggregate of barstar at low pH. *Biochemistry* 41, 9885–9899.
- Gast, K., Modler, A. J., Damaschun, H., Krober, R., Lutsch, G., Zirwer, D., Golbik, R., and Damaschun, G. (2003) Effect of environmental conditions on aggregation and fibril formation of barstar. *Eur. Biophys. J.* 32, 710–723.
- Jha, A., Udgaonkar, J. B., and Krishnamoorthy, G. (2009) Characterization of the heterogeneity and specificity of interpeptide interactions in amyloid protofibrils by measurement of site-specific fluorescence anisotropy decay kinetics. *J. Mol. Biol.* 393, 735–752.
- Sridevi, K., and Udgaonkar, J. B. (2003) Surface expansion is independent of and occurs faster than core solvation during the unfolding of barstar. *Biochemistry* 42, 1551–1563.
- Takeuchi, S., and Tahara, T. (1997) Ultrafast fluorescence study on the excited singlet-state dynamics of all-trans-retinal. *J. Phys. Chem. A* 101, 3052–3060.
- Iwamura, M., Takeuchi, S., and Tahara, T. (2007) Real-time observation of the photoinduced structural change of bis(2,9-dimethyl-1,10-phenanthroline)copper(I) by femtosecond fluorescence spectroscopy: A realistic potential curve of the Jahn-Teller distortion. *J. Am. Chem. Soc.* 129, 5248–5256.
- Fee, R. S., and Maroncelli, M. (1994) Estimating the time-zero spectrum in time-resolved emission measurements of solvation dynamics. *Chem. Phys.* 183, 235–247.
- Prendergast, F. G., Meyer, M., Carlson, G. L., Iida, S., and Potter, J. D. (1983) Synthesis, spectral properties, and use of 6-acryloyl-2-dimethylaminonaphthalene (acrylodan). A thiol-selective, polarity-sensitive fluorescent probe. *J. Biol. Chem.* 258, 7541–7544.
- Guha, S., Sahu, K., Roy, D., Mondal, S. K., Roy, S., and Bhattacharyya, K. (2005) Slow solvation dynamics at the active site of an enzyme: implications for catalysis. *Biochemistry* 44, 8940–8947.
- Zhao, L., Pal, S. K., Xia, T., and Zewail, A. H. (2004) Dynamics of ordered water in interfacial enzyme recognition: bovine pancreatic phospholipase A2. *Angew. Chem., Int. Ed. Engl.* 43, 60–63.
- Adhikary, R., Barnes, C. A., and Petrich, J. W. (2009) Solvation dynamics of the fluorescent probe PRODAN in heterogeneous environments: contributions from the locally excited and charge-transferred states. *J. Phys. Chem. B* 113, 11999–12004.
- Dey, S., Adhikari, A., Das, D. K., Sasmal, D. K., and Bhattacharyya, K. (2009) Femtosecond solvation dynamics in a micron-sized aggregate of an ionic liquid and P123 triblock copolymer. *J. Phys. Chem. B* 113, 959–965.

27. Kamal, J. K., Zhao, L., and Zewail, A. H. (2004) Ultrafast hydration dynamics in protein unfolding: human serum albumin. *Proc. Natl. Acad. Sci. U.S.A.* *101*, 13411–13416.
28. Dupradeau, F. Y., Case, D. A., Yu, C., Jimenez, R., and Romesberg, F. E. (2005) Differential solvation and tautomer stability of a model base pair within the minor and major grooves of DNA. *J. Am. Chem. Soc.* *127*, 15612–15617.
29. Pal, S. K., Peon, J., and Zewail, A. H. (2002) Biological water at the protein surface: dynamical solvation probed directly with femtosecond resolution. *Proc. Natl. Acad. Sci. U.S.A.* *99*, 1763–1768.
30. Pal, S. K., and Zewail, A. H. (2004) Dynamics of water in biological recognition. *Chem. Rev.* *104*, 2099–2123.
31. Swaminathan, R., Nath, U., Udgaonkar, J. B., Periasamy, N., and Krishnamoorthy, G. (1996) Motional dynamics of a buried tryptophan reveals the presence of partially structured forms during denaturation of barstar. *Biochemistry* *35*, 9150–9157.
32. Rami, B. R., Krishnamoorthy, G., and Udgaonkar, J. B. (2003) Dynamics of the core tryptophan during the formation of a productive molten globule intermediate of barstar. *Biochemistry* *42*, 7986–8000.
33. Eftink, M. R. (1991) Topics in Fluorescence Spectroscopy, Vol. 2, Plenum Press, New York.
34. Hass, M. A., Thuesen, M. H., Christensen, H. E., and Led, J. J. (2004) Characterization of micro-ms dynamics of proteins using a combined analysis of ¹⁵N NMR relaxation and chemical shift: conformational exchange in plastocyanin induced by histidine protonations. *J. Am. Chem. Soc.* *126*, 753–765.
35. Blanco-Rodriguez, A. M., Busby, M., Ronayne, K., Towrie, M., Gradinaru, C., Sudhamsu, J., Sykora, J., Hof, M., Zalis, S., Di Bilio, A. J., Crane, B. R., Gray, H. B., and Vlcek, A., Jr. (2009) Relaxation dynamics of *Pseudomonas aeruginosa* Re(I)(CO)₃(α-diimine)-(HisX)⁺ (X = 83, 107, 109, 124, 126)Cu(II) azurins. *J. Am. Chem. Soc.* *131*, 11788–11800.
36. Zang, C., Stevens, J. A., Link, J. J., Guo, L., Wang, L., and Zhong, D. (2009) Ultrafast proteinquake dynamics in cytochrome *c*. *J. Am. Chem. Soc.* *131*, 2846–2852.
37. Nilsson, L., and Halle, B. (2005) Molecular origin of time-dependent fluorescence shifts in proteins. *Proc. Natl. Acad. Sci. U.S.A.* *102*, 13867–13872.
38. Nandi, N., and Bagchi, B. (1997) Dielectric relaxation of biological water. *J. Phys. Chem. B* *101*, 10954–10961.
39. Nandi, N., Bhattacharyya, K., and Bagchi, B. (2000) Dielectric relaxation and solvation dynamics of water in complex chemical and biological systems. *Chem. Rev.* *100*, 2013–2046.
40. Jimenez, R., Fleming, G. R., Kumar, P. V., and Maroncelli, M. (1994) Femtosecond solvation dynamics of water. *Nature* *369*, 471–473.
41. Jordanides, X. J., Lang, M. J., Song, X. Y., and Fleming, G. R. (1999) Solvation dynamics in protein environments studied by photon echo spectroscopy. *J. Phys. Chem. B* *103*, 7995–8005.
42. Bagchi, B. (2005) Water dynamics in the hydration layer around proteins and micelles. *Chem. Rev.* *105*, 3197–3219.
43. Halle, B. (2004) Protein hydration dynamics in solution: a critical survey. *Philos. Trans. R. Soc. London, Ser. B* *359*, 1207–1223 (discussion 1223–1204, 1323–1208).
44. Maroncelli, M., and Fleming, G. R. (1987) Picosecond solvation dynamics of coumarin-153—the importance of molecular aspects of solvation. *J. Chem. Phys.* *86*, 6221–6239.
45. Frauenfelder, H., Fenimore, P. W., and Young, R. D. (2007) Protein dynamics and function: insights from the energy landscape and solvent slaving. *IUBMB Life* *59*, 506–512.
46. Lubchenko, V., Wolynes, P. G., and Frauenfelder, H. (2005) Mosaic energy landscapes of liquids and the control of protein conformational dynamics by glass-forming solvents. *J. Phys. Chem. B* *109*, 7488–7499.
47. Frauenfelder, H., Fenimore, P. W., Chen, G., and McMahon, B. H. (2006) Protein folding is slaved to solvent motions. *Proc. Natl. Acad. Sci. U.S.A.* *103*, 15469–15472.
48. Cohen, B. E., McAnaney, T. B., Park, E. S., Jan, Y. N., Boxer, S. G., and Jan, L. Y. (2002) Probing protein electrostatics with a synthetic fluorescent amino acid. *Science* *296*, 1700–1703.
49. Bandyopadhyay, S., Chakraborty, S., Balasubramanian, S., and Bagchi, B. (2005) Sensitivity of polar solvation dynamics to the secondary structures of aqueous proteins and the role of surface exposure of the probe. *J. Am. Chem. Soc.* *127*, 4071–4075.
50. Sen, P., Mukherjee, S., Dutta, P., Halder, A., Mandal, D., Banerjee, R., Roy, S., and Bhattacharyya, K. (2003) Solvation dynamics in the molten globule state of a protein. *J. Phys. Chem. B* *107*, 14563–14568.